

# LightSBB-M: Bridging Schrödinger and Bass for Generative Diffusion Modeling

Alexandre ALOUADI<sup>1</sup> Pierre HENRY-LABORDERE<sup>2</sup> Grégoire LOEPER<sup>3</sup> Othmane MAZHAR<sup>4</sup>  
Huyêñ PHAM<sup>5</sup> Nizar TOUZI<sup>6</sup>

## Abstract

The Schrödinger Bridge and Bass (SBB) formulation, which jointly controls drift and volatility, is an established extension of the classical Schrödinger Bridge (SB). Building on this framework, we introduce **LightSBB-M**, an algorithm that computes the optimal SBB transport plan in only a few iterations. The method exploits a dual representation of the SBB objective to obtain analytic expressions for the optimal drift and volatility, and it incorporates a tunable parameter  $\beta > 0$  that interpolates between pure drift (the Schrödinger Bridge) and pure volatility (Bass martingale transport). We show that LightSBB-M achieves the lowest 2-Wasserstein distance on synthetic datasets against state-of-the-art SB and diffusion baselines with up to 32% improvement. We also illustrate the generative capability of the framework on an unpaired image-to-image translation task (*adult*  $\rightarrow$  *child* faces in FFHQ). These findings demonstrate that **LightSBB-M** provides a scalable, high-fidelity SBB solver that outperforms existing SB and diffusion baselines across both synthetic and real-world generative tasks. The code is available at <https://github.com/alexouadi/LightSBB-M>.

## 1. Introduction

Stochastic-process-based generative modeling has recently gained significant attention, notably through diffusion models and Schrödinger Bridge (SB) formulations, which construct a controlled stochastic dynamics transporting a source distribution  $\mu_0$  to a target distribution  $\mu_T$  (Schrödinger,

<sup>1</sup>École Polytechnique & BNP PARIBAS <sup>2</sup>Qube RT  
<sup>3</sup>BNP PARIBAS <sup>4</sup>Université Paris Cité <sup>5</sup>École Polytechnique <sup>6</sup>New York University. Correspondence to: Alexandre ALOUADI <[alexandre.alouadi@bnpparibas.com](mailto:alexandre.alouadi@bnpparibas.com)>, Huyêñ PHAM <[huyen.pham@polytechnique.edu](mailto:huyen.pham@polytechnique.edu)>.

Preprint. January 28, 2026.

1932; Léonard, 2014; De Bortoli et al., 2021). By minimizing the relative entropy with respect to a Brownian prior, SB establishes deep connections between optimal transport, stochastic control, and score-based learning. However, the classical SB framework relies on a fixed volatility and requires finite entropy with respect to the Wiener measure, which limits its applicability for heavy-tailed or singular target distributions.

Bass martingale transport provides an alternative formulation by optimizing over volatility while enforcing a zero drift constraint (Bass, 1983; Backhoff et al., 2025). While this approach allows for greater flexibility on the marginals, it departs from diffusion-based generative mechanisms and lacks an explicit drift control. The Schrödinger-Bass Bridge (SBB) problem unifies these two paradigms by jointly optimizing over drift and volatility, introducing a parameter  $\beta > 0$  that interpolates between the classical SB limit ( $\beta \rightarrow \infty$ ) and the Bass martingale transport regime ( $\beta \rightarrow 0$ ).

Despite its theoretical appeal, the SBB problem has received limited attention from a computational perspective, especially in high-dimensional generative modeling. Extending existing SB solvers to this setting is challenging due to the presence of stochastic volatility and implicit transport maps.

In this work, we introduce **LightSBB-M**, a simulation-efficient algorithm for solving the SBB problem. Leveraging a dual formulation of SBB and recent advances in Light Schrödinger Bridge matching (Gushchin et al., 2024), our approach yields analytic expressions for the optimal drift and volatility and converges in only a few iterations.

Our main contributions are summarized as follows:

- We propose a practical and scalable algorithm to compute the optimal Schrödinger-Bass Bridge, enabling efficient generative modeling with jointly learned drift and volatility.
- We derive explicit and tractable expressions for the optimal SBB controls, allowing simulation-free sampling and avoiding costly SDE discretization.

- We provide extensive numerical experiments on synthetic and high-dimensional datasets, demonstrating improved transport accuracy and generative performance compared to state-of-the-art Schrödinger Bridge and diffusion-based baselines.

This work advances the interface between optimal transport theory and modern generative modeling by making stochastic-volatility transport computationally tractable at scale. Beyond images, the framework opens new directions for generative modeling under distributional constraints, heavy-tailed data, and time-series with heteroskedasticity—settings that remain challenging for standard diffusion models.

## 2. Background

### 2.1. The Schrödinger Bridge Problem

In this section, we recall the formulation of the Schrödinger Bridge Problem (SBP) (Schrödinger, 1932). Let  $\Omega = \mathcal{C}([0, T], \mathbb{R}^d)$  denote the space of continuous  $\mathbb{R}^d$ -valued paths on  $[0, T]$ , with  $T < \infty$ . Let  $X = (X_t)_{t \in [0, T]}$  be the canonical process, and let  $\mathcal{P}(\Omega)$  denote the set of probability measures on the path space  $\Omega$ . For  $\mathbb{P} \in \mathcal{P}(\Omega)$ ,  $\mathbb{P}_t = X_t \# \mathbb{P}$  is the marginal law of  $X_t$  under  $\mathbb{P}$  at time  $t$ .

Let  $\mu_0$  and  $\mu_T$  be two probability distributions on  $\mathbb{R}^d$ . Let  $\mathbb{W}^\varepsilon$  denote the Wiener measure with variance  $\varepsilon > 0$  on  $\Omega$ , which represents the prior belief about the system dynamics before observing data. The SBP is then formulated as the following entropy-minimization problem:

$$\mathbb{P}^* \in \operatorname{argmin}_{\mathbb{P}} \left\{ \text{KL}(\mathbb{P} \parallel \mathbb{W}^\varepsilon) : \mathbb{P} \in \mathcal{P}(\Omega), \mathbb{P}_0 = \mu_0, \mathbb{P}_T = \mu_T \right\}, \quad (1)$$

where  $\text{KL}(\mathbb{P} \parallel \mathbb{W}^\varepsilon) = \mathbb{E}_{\mathbb{P}} \left[ \ln \frac{d\mathbb{P}}{d\mathbb{W}^\varepsilon} \right]$  denotes the Kullback–Leibler (KL) divergence between  $\mathbb{P}$  and  $\mathbb{W}$ .

If  $\text{KL}(\mathbb{P} \parallel \mathbb{W}^\varepsilon) < \infty$ , then by Girsanov's theorem, the optimization problem (1) admits a stochastic control formulation. Specifically, one seeks an  $\mathbb{R}^d$ -valued control process  $\alpha$  satisfying  $\mathbb{E}_{\mathbb{P}} \left[ \int_0^T \|\alpha_t\|^2 dt \right] < \infty$  such that

$$\alpha^* \in \operatorname{argmin}_{\alpha} \left\{ \mathbb{E}_{\mathbb{P}} \left[ \int_0^T \|\alpha_t\|^2 dt \right] : X_0 \sim \mu_0, X_T \sim \mu_T \right\}, \quad (2)$$

with the controlled dynamics  $dX_t = \alpha_t dt + \sqrt{\varepsilon} dW_t$ ,  $W$  a Brownian motion under  $\mathbb{P}$ .

The associated path measure  $\mathbb{P}^{SB} \in \mathcal{P}(\Omega)$  is the one closest to the Wiener path measure  $\mathbb{W}^\varepsilon$  in terms of KL divergence, and disintegrated as  $\mathbb{P}^{SB} = \pi_{0,T}^{SB} \mathbb{W}_{[0,T]}^\varepsilon$ , where  $\pi_{0,T}^{SB}$  denotes the optimal coupling of the following static Entropic Optimal Transport (EOT) problem:

$$\operatorname{argmin}_{\pi \in \mathcal{P}(\mathbb{R}^d \times \mathbb{R}^d)} \left\{ \mathbb{E}_{\pi} [|X_0 - X_T|^2] - 2T\varepsilon \mathcal{H}(\pi) : \pi_0 = \mu_0, \pi_T = \mu_T \right\},$$

where  $\mathcal{H}(\pi)$  denotes the entropy, and  $\mathbb{W}_{[0,T]}^\varepsilon$  is the law of the Brownian bridge between times 0 and  $T$ . The optimal EOT plan takes the form  $\pi_{0,T}^{SB}(x_0, x_T) = \nu_0(x_0) e^{-\frac{|x_0 - x_T|^2}{2\varepsilon T}} e^{\psi(x_T)}$  where the so-called *potentials*  $\nu_0$  and  $\psi = \log h_T$  satisfy the Schrödinger system under the marginal constraints:

$$\begin{cases} \mu_T = h_T \nu_T, & \nu_T(x) = \nu_0 * \mathcal{N}_{\varepsilon T}(x), \\ \mu_0 = h_0 \nu_0, & h_0(x) = h_T * \mathcal{N}_{\varepsilon T}(x). \end{cases} \quad (3)$$

where  $\mathcal{N}_{\sigma^2}$  denotes the Gaussian distribution with variance  $\sigma^2$ . Finally, the optimal drift is given by the score function  $\alpha^*(t, x) = \varepsilon \nabla_x \log h_t(x)$ ,  $(t, x) \in [0, T) \times \mathbb{R}^d$  where  $h_t = h_T * \mathcal{N}_{\varepsilon(T-t)}$ .

### 2.2. Diffusion Schrödinger Bridge for Generative Modeling

Given samples from  $\mu_0$  and  $\mu_T$ , the objective is to learn the solution of the SBP in order to generate new samples from  $\mu_T$  given unseen samples from  $\mu_0$ . To achieve this, one may either learn the path measure  $\mathbb{P}^{SB} = \pi_{0,T}^{SB} \mathbb{W}_{[0,T]}^\varepsilon$  solving (1), where the Brownian bridge component  $\mathbb{W}_{[0,T]}^\varepsilon$  is known and only the optimal coupling  $\pi_{0,T}^{SB}$  needs to be estimated, or alternatively learn the optimal drift  $\alpha^*$  solving (2), and then simulate the controlled dynamics  $dX_t = \alpha_t^* dt + \sqrt{\varepsilon} dW_t$ , starting from  $X_0 \sim \mu_0$ , to obtain new samples  $X_T \sim \mu_T$ . Several recent and competitive *Diffusion Schrödinger Bridge* (DSB) solvers have been proposed to address this learning problem.

#### 2.2.1. SINKHORN ALGORITHM

Recall the optimal plan admits the separable form

$$\pi_{0,T}^{SB}(x_0, x_T) = \nu_0(x_0) e^{-\frac{|x_0 - x_T|^2}{2\varepsilon T}} e^{\psi(x_T)},$$

where the Schrödinger potentials  $(\nu_0, \psi)$  solve the Schrödinger system (3), with  $\psi = \log h_T$ .

The Sinkhorn algorithm computes  $(\nu_0, h_T)$  by iteratively enforcing the marginal constraints, see e.g. (Léonard, 2014; Peyré & Cuturi, 2019). Starting from an initial guess  $h_T^{(0)}$ , the iterations read

$$\begin{cases} \nu_0^{(k+1)}(x) = \frac{\mu_0(x)}{h_0^{(k)}(x)}, & h_0^{(k)} = h_T^{(k)} * \mathcal{N}_{\varepsilon T}, \\ h_T^{(k+1)}(x) = \frac{\mu_T(x)}{\nu_T^{(k+1)}(x)}, & \nu_T^{(k+1)} = \nu_0^{(k+1)} * \mathcal{N}_{\varepsilon T}. \end{cases}$$

At convergence, one recovers the SB coupling  $\pi_{0,T}^{SB}$  and the associated SB drift  $\alpha^*(t, x) = \varepsilon \nabla_x \log h_t(x)$  with  $h_t = h_T * \mathcal{N}_{\varepsilon(T-t)}$ , see (Föllmer, 1988; Léonard, 2014).

While Sinkhorn is simulation-free and easy to implement, it suffers from important drawbacks in practice. Its reliance on

repeated Gaussian convolutions makes it poorly scalable in high dimension and numerically unstable in the small-noise regime  $\varepsilon \rightarrow 0$  (Peyré & Cuturi, 2019; De Bortoli et al., 2021). Moreover, Sinkhorn only provides the endpoint coupling and Schrödinger potentials, and does not yield a parametric or dynamic representation of the SB process, which limits its applicability to generative modeling (Shi et al., 2023).

### 2.2.2. ITERATIVE MARKOVIAN FITTING

We recall that  $\mathbb{P}^{SB}$  is the unique measure satisfying the boundary conditions  $\mathbb{P}_0^{SB} = \pi_0$  and  $\mathbb{P}_T^{SB} = \pi_T$  such that  $\mathbb{P}^{SB}$  is Markovian and  $\mathbb{P}_{[0,T]}^{SB} = \mathbb{W}_{[0,T]}^\varepsilon$  simultaneously (Léonard, 2014). If the last condition is verified, we say that  $\mathbb{P}^{SB} \in \mathcal{R}(\mathbb{W}^\varepsilon)$  the reciprocal class of the reference measure  $\mathbb{W}^\varepsilon$  (Shi et al., 2023). In other words, given an initial point  $x_0$  and a terminal point  $x_T$ , the law of the process  $X$  is a Brownian motion. The *Iterative Markovian Fitting* (IMF) algorithm (Shi et al., 2023) provides an alternative methodology for computing  $\mathbb{P}^{SB}$ . It constructs a sequence of path measures  $(\mathbb{P}^n)_{n \in \mathbb{N}}$  by alternating between two projections:

$$\begin{cases} \mathbb{P}^{2n+1} = \text{proj}_{\mathcal{M}}(\mathbb{P}^{2n}), \\ \mathbb{P}^{2n+2} = \text{proj}_{\mathcal{R}(\mathbb{W}^\varepsilon)}(\mathbb{P}^{2n+1}), \end{cases}$$

initialized with a measure  $\mathbb{P}^0 \in \mathcal{R}(\mathbb{W}^\varepsilon)$  satisfying the boundary conditions  $\mathbb{P}_0^0 = \pi_0$  and  $\mathbb{P}_T^0 = \pi_T$ . Here,  $\mathcal{M}$  denotes the space of Markov measures. The IMF iterates preserve the marginal constraints  $\mathbb{P}_0^n = \pi_0$  and  $\mathbb{P}_T^n = \pi_T$  for all  $n$  and converges to the unique SB,  $\mathbb{P}^* = \mathbb{P}^{SB}$ . However, this method is not simulation-free and can suffer from error accumulation across iterations if the Markovian projection step is not learned perfectly.

### 2.2.3. LIGHTSB-M: LIGHT SCHRÖDINGER BRIDGE MATCHING

The LightSB-M (Gushchin et al., 2024) method solves the SB problem via a single, *optimal projection* step based on a new characterization of SB. Let  $\pi \in \Pi(\mu_0, \mu_T)$  with  $\Pi(\mu_0, \mu_T)$  the set of all transport plans between  $\mu_0$  and  $\mu_T$ , and  $\mathbb{P}^\pi = \pi \mathbb{W}_{[0,T]}^\varepsilon$  its reciprocal process. Then (Gushchin et al., 2024)

$$\mathbb{P}^{SB} = \underset{\mathbb{Q} \in \mathcal{S}(\mu_0)}{\text{argmin}} \text{KL}(\mathbb{P}^\pi | \mathbb{Q}), \quad (4)$$

where  $\mathcal{S}(\mu_0)$  is the set of SB processes starting from  $\mu_0$ . From the separable form of optimal EOT, the optimal plan associated to a process in  $\mathcal{S}(\mu_0)$  can be written in the disintegrated form:

$$\pi_\varphi(x_0, x_T) = \mu_0(x_0) \underbrace{\frac{e^{<x_0, x_T>/\varepsilon} \varphi(x_T)}{c_\varphi(x_0)}}_{\pi_\varphi(x_T | x_0)}, \quad (5)$$

where  $c_\varphi(x_0) := \int e^{<x_0, x_T>/\varepsilon} \varphi(x_T) dx_T$ , and  $\varphi$  is the adjusted potential. Setting  $\mathbb{Q}_\varphi := \pi_\varphi \mathbb{W}_{[0,T]}^\varepsilon \in \mathcal{S}(\mu_0)$  yields a tractable objective for (4) (Gushchin et al., 2024)

$$\text{KL}(\mathbb{P}^\pi | \mathbb{Q}_\varphi) = \frac{1}{2} \underbrace{\mathbb{E}^{\mathbb{P}^\pi} \left[ \left\| \alpha_\varphi(t, X_t) - \frac{X_T - X_t}{T - t} \right\|^2 \right]}_{\text{DSM}(\varphi)} + C(\pi),$$

where  $\alpha_\varphi$  is the score-drift of  $\mathbb{Q}_\varphi$ . We are then led to minimize over  $\varphi$  the denoising score matching loss  $\text{DSM}(\varphi)$  via stochastic gradient descent. In practice, one parametrizes  $\varphi$  by a mixture of Gaussian densities such that  $\alpha_\varphi$  is analytic and requires no neural network (Korotin et al., 2024). Once  $\varphi^*$  is learnt, we sample  $X_0 \sim \mu_0$ ,  $X_T \sim \pi_{\varphi^*}(\cdot | X_0) \sim \mu_T$ , and so we do not have to solve the associated SDE.

## 3. Bridging Schrödinger and Bass

The Schrödinger–Bass (SBB) problem is an extension of the classical SB problem by jointly optimizing over both drift and volatility. It is introduced and studied in (Alouadi et al., 2026). Given two distributions  $\mu_0, \mu_T \in \mathcal{P}(\mathbb{R}^d)$ , the goal is to minimize, over  $\mathbb{P} \in \mathcal{P}(\mu_0, \mu_T) = \{ \mathbb{P} \in \mathcal{P}(\Omega) : X_0 \stackrel{\mathbb{P}}{\sim} \mu_0, X_T \stackrel{\mathbb{P}}{\sim} \mu_T \}$ , the quadratic cost:

$$J(\mathbb{P}) = \mathbb{E}_{\mathbb{P}} \left[ \int_0^T \underbrace{\|\alpha_t\|^2 + \beta \|\sigma_t - \sqrt{\varepsilon} I_d\|^2}_{H_\beta(\alpha_t, \sigma_t)} dt \right], \quad (6)$$

for some  $\beta > 0$ , where  $(\alpha, \sigma)$  is the drift/volatility of  $X$  under  $\mathbb{P}$ , i.e.,  $dX_t = \alpha_t dt + \sigma_t dW_t$ . This problem is denoted by  $\text{SBB}(\mu_0, \mu_T) := \inf_{\mathbb{P} \in \mathcal{P}(\mu_0, \mu_T)} J(\mathbb{P})$ .

Note that as  $\beta \rightarrow \infty$ , the volatility  $\sigma$  is constrained to equal  $I_d$ , recovering the classical SB problem. Conversely, dividing (6) by  $\beta$  and letting  $\beta \rightarrow 0$  forces the drift term  $\alpha$  to vanish, yielding the Bass martingale transport problem. In other words, the parameter  $\beta$  controls the relative weight of drift versus volatility, interpolating between these two well-known cases.

### 3.1. Dual Representation of the Primal SBB

The primal problem  $\text{SBB}(\mu_0, \mu_T)$  admits a dual representation, which consists of maximizing over a suitable class of functions  $(v, \psi)$  the Lagrangian functional

$$L_{\mu_0, \mu_T}(\psi, v) = \int \psi(x) \mu_T(dx) - \int v(0, x) \mu_0(dx),$$

where  $v$  is the value function of the unconstrained stochastic control problem with Bellman equation:

$$\begin{cases} \partial_t v + H_\beta^*(\nabla_x v, D_x^2 v) = 0, & \text{on } [0, T] \times \mathbb{R}^d, \\ v(T, \cdot) = \psi, & \text{on } \mathbb{R}^d, \end{cases} \quad (7)$$

with  $H_\beta^*$  denoting the Fenchel–Legendre transform of  $H_\beta$ , explicitly given by

$$H_\beta^*(p, q) = \frac{1}{2}|p|^2 + \frac{\varepsilon\beta}{2}I_d : \left( \left( I_d - \frac{q}{\beta} \right)^{-1} - I_d \right),$$

for  $(p, q) \in \mathbb{R}^d \times \mathbb{S}_+^d$  such that  $q < \beta I_d$ . Assuming that  $\text{SBB}(\mu_0, \mu_T) < \infty$ , we have:

- **Attainment of the primal problem:** there exists  $(\alpha^*, \sigma^*) \leftrightarrow \mathbb{P}^{\text{SBB}}$  attaining the infimum in  $\text{SBB}(\mu_0, \mu_T)$ , in feedback form:  $\alpha_t^* = a^*(t, X_t)$ ,  $\sigma_t^* = \vartheta^*(t, X_t)$ .
- **Duality relation:** we have

$$\text{SBB}(\mu_0, \mu_T) = \sup_{\substack{\psi \in C^2 \cap C_b^\infty \cap L^1(\mu_T), v \in C_b^{1,2}, \\ D_x^2 v < \beta I_d, \psi = v(T, \cdot), \\ \partial_t v + H_\beta^*(\nabla_x v, D_x^2 v) = 0}} L_{\mu_0, \mu_T}(\psi, v) \quad (8)$$

- **Duality on the control:**

When  $\mu_0$  and  $\mu_T$  have finite second moment, and if  $\beta > \frac{1}{T}$ , then the supremum in the dual problem is attained at  $(v^*, \psi^*)$ , and the optimal feedback policies are given by

$$\begin{cases} a^*(t, x) = \nabla_x v^*(t, x), & (t, x) \in [0, T) \times \mathbb{R}^d, \\ \vartheta^*(t, x) = \sqrt{\varepsilon} \left( I_d - \frac{D_x^2 v^*(t, x)}{\beta} \right)^{-1}. \end{cases}$$

### 3.2. SBB System

One can exploit the quadratic form of the SBB criterion to reduce the dual problem to the maximization over the potential  $\psi \in C^2 \cap C_b^\infty \cap L^1(\mu_T)$ , subject to  $D_x^2 \psi < \beta I_d$ , of the Donsker–Varadhan type functional:

$$\int \psi d\mu_T - \int \underbrace{\mathcal{T}_\beta^+ \left[ \varepsilon \log \int e^{\mathcal{T}_\beta^-[\psi](\cdot+z)} \mathcal{N}_{\varepsilon T}(dz) \right] (x)}_v \mu_0(dx),$$

where  $\mathcal{T}_\beta^\pm$  are the **quadratic inf/sup convolution** operators:

$$\begin{cases} \mathcal{T}_\beta^+[\phi](x) := \inf_{y \in \mathbb{R}^d} \left[ \phi(y) + \frac{\beta}{2} |x - y|^2 \right], & x \in \mathbb{R}^d, \\ \mathcal{T}_\beta^-[\psi](y) := \sup_{x \in \mathbb{R}^d} \left[ \psi(x) - \frac{\beta}{2} |x - y|^2 \right], & y \in \mathbb{R}^d. \end{cases}$$

This leads to the SBB system, where a potential  $\psi^*$  (or  $\phi^* = \mathcal{T}_\beta^-[\psi^*] = \log h_T^*$ ) of the dual SBB problem satisfies:

$$\begin{cases} \mathcal{Y}_T \# \mu_T = h_T^* \nu_T, & \nu_T = \nu_0 * \mathcal{N}_{\varepsilon T} \\ \mathcal{Y}_0 \# \mu_0 = h_0^* \nu_0, & h_0^* = h_T^* * \mathcal{N}_{\varepsilon T} \end{cases}$$

where  $\#$  is the pushforward operator, and the transport map  $\mathcal{Y}_t$  is defined as :

$$\mathcal{Y}_t = (\nabla_y \Phi_t)^{-1}, \quad \Phi_t(y) = \frac{|y|^2}{2} + \frac{1}{\beta} \varepsilon \log h_t^*(y),$$

which is an increasing (convex) function from  $\mathbb{R}^d$  into  $\mathbb{R}^d$  for any  $t \in [0, T]$ . Note that when  $\beta \rightarrow \infty$ ,  $\mathcal{Y} = \text{Id}$  and we recover the Schrödinger system. Conversely, when  $\beta \rightarrow 0$ ,  $h^*$  is constant and we recover the Bass system. The optimal drift and volatility of SBB are given by

$$\begin{cases} \alpha_t^* = \varepsilon \nabla_y \log h_t^*(\mathcal{Y}_t(X_t)), \\ \sigma_t^* = \sqrt{\varepsilon} D_y^2 \Phi_t(\mathcal{Y}_t(X_t)), \end{cases} \quad t \in [0, T].$$

If we define the process

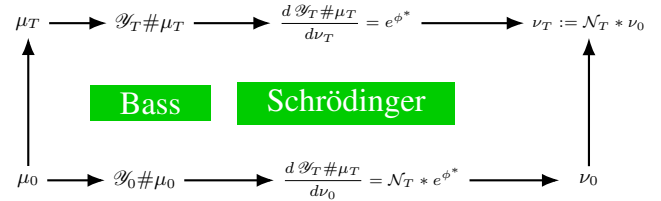
$$Y_t = \mathcal{Y}_t(X_t) = X_t - \frac{1}{\beta} \varepsilon \nabla_y \log h_t^*(\mathcal{Y}_t(X_t)), \quad t \in [0, T], \quad (9)$$

and the change of measure  $\frac{d\mathbb{Q}^*}{d\mathbb{P}^{\text{SBB}}} \Big|_{\mathcal{F}_t} = \frac{1}{h_t^*(Y_t)}$ ,  $t \in [0, T]$  (which is indeed a  $\mathbb{P}^{\text{SBB}}$ -martingale with expectation 1 by the SBB system), then

- $(Y_t)$  is a Brownian motion with volatility  $\sqrt{\varepsilon}$  under  $\mathbb{Q}^*$  with initial law  $\nu_0$ .
- $X_t = \mathcal{Y}_t^{-1}(Y_t) = Y_t + \frac{\varepsilon}{\beta} \nabla_y \log h_t^*(Y_t)$ ,  $t \in [0, T]$ , is a stretched Brownian motion under  $\mathbb{Q}^*$ .
- The dynamics under  $\mathbb{P}^{\text{SBB}}$  are:

$$\begin{cases} dX_t = D_y^2 \Phi_t(Y_t) dY_t, \\ dY_t = \varepsilon \nabla_y \log h_t^*(Y_t) dt + \sqrt{\varepsilon} dW_t, \end{cases} \quad t \in [0, T].$$

In other words,  $\mathbb{P}^{\text{SBB}}$  is the Bass transport of a SB, i.e., a stretched SB. The SBB system can be visualized in the figure below.



### 4. Generative Modeling with SBB

To generate new samples from  $\mu_T$  via the learned SBB system, one could directly simulate

$$\begin{aligned} dX_t = & \varepsilon \nabla_y \log h_t^*(\mathcal{Y}_t(X_t)) dt \\ & + \sqrt{\varepsilon} D_y^2 \Phi_t(\mathcal{Y}_t(X_t)) dW_t, \quad X_0 \sim \mu_0, \end{aligned}$$

using an SDE solver (e.g., the Euler–Maruyama scheme) to obtain  $X_T \sim \mu_T$ . However, this requires computing the inverse of a Hessian matrix, which can be challenging in high dimensions. To overcome this, one can instead generate the process  $Y = \mathcal{Y}(X)$  as a DSB:

$$dY_t = \varepsilon \nabla_y \log h_t^*(Y_t) dt + \sqrt{\varepsilon} dW_t,$$

with  $Y_0 \sim \mathcal{Y}_0 \# \mu_0$  and  $Y_T \sim \mathcal{Y}_T \# \mu_T$ , and score drift

$$s_t^*(y) = \varepsilon \nabla_y \log h_t^*(y).$$

Then,  $X_T$  can be recovered via

$$X_T = \mathcal{Y}_T^{-1}(Y_T) = Y_T + \frac{1}{\beta} s_T^*(Y_T) \sim \mu_T.$$

#### 4.1. Training

As Section 2.2.3 provides an efficient way to solve the SB between  $\mathcal{Y}_0 \# \mu_0$  and  $\mathcal{Y}_T \# \mu_T$ , it remains to learn the transport map  $\mathcal{Y}$ . Exploiting that  $\mathcal{Y}_t = \mathcal{X}_t^{-1}$  with

$$\mathcal{X}_t(y) = y + \frac{1}{\beta} s_t^*(y),$$

we can learn the inverse of  $\mathcal{X}$  using a neural network  $\mathcal{Z}_{\tilde{\theta}}$  to obtain  $\mathcal{Y}$ , avoiding the need to solve the fixed point (9). We then introduce LightSBB-M (Algorithm 1) to efficiently solve the SBB problem as follows.

Let  $\theta = \{\alpha_j, r_j, \Sigma_j\}_{j=1}^J$  denote the parameters of a Gaussian-mixture potential  $v_\theta$ , and  $\tilde{\theta}$  the parameters of the neural network  $Z_{\tilde{\theta}}$ . Initialize  $\phi^0 = 0$ , hence  $\mathcal{Y}^0 = \mathcal{Z}_{\tilde{\theta}}^0 = I_d$ . Then, for  $0 \leq k \leq K$ :

1. **Endpoint sampling.** Draw endpoint pairs  $(y_0, y_T)$  from a coupling of  $(p_0^k, p_T^k)$ , where  $p_t^k = d(\mathcal{Y}_t^k \# \mu_t)/dy$ , using

$$\begin{cases} \mathcal{Y}_0^k(x_0) = y_0 = \mathcal{Z}_{\tilde{\theta}}^k(0, x_0), & x_0 \sim \mu_0, \\ \mathcal{Y}_T^k(x_T) = y_T = \mathcal{Z}_{\tilde{\theta}}^k(T, x_T), & x_T \sim \mu_T. \end{cases}$$

2. **Bridge sampling.** For  $t \sim \mathcal{U}[0, T]$  and  $Z \sim \mathcal{N}(0, I_d)$ , sample  $y_t \sim \mathbb{W}_{|y_0, y_T}^\varepsilon$  as an intermediate point from the Brownian bridge:

$$y_t = \frac{T-t}{T} y_0 + \frac{t}{T} y_T + \sigma_t \sqrt{\varepsilon} Z, \quad \sigma_t^2 = \frac{t(T-t)}{T}. \quad (10)$$

3. **Regression step on  $\theta$ .** Update  $\theta^k$  by minimizing the bridge-matching loss

$$\mathcal{L}(\theta^k) = \mathbb{E}_{t \sim \mathcal{U}(0, T)} \mathbb{E}_{y_T \sim p_T, y_t \sim \mathbb{W}_{|y_0, y_T}^\varepsilon} \left[ \left\| s_\theta^k(t, y_t) - \frac{y_T - y_t}{T-t} \right\|_2^2 \right], \quad (11)$$

which is the KL projection onto the set of SBs, ensuring that the learned drift coincides with the true SB drift.

#### Algorithm 1 LightSBB-M Training Algorithm

---

**Input:** Samples  $(x_0^m, x_T^m)_{m \leq M} \sim (\mu_0, \mu_T)$ ,  $\theta = \{\alpha_j, \mu_j, \Sigma_j\}_{j \leq J}$ ,  $\tilde{\theta}, \beta > 0, K > 0$   
**Initialization:** Start with  $\mathcal{Y}^0 = I_d$  and  $\mathcal{Z}_{\tilde{\theta}}^0 = I_d$   
**for**  $k = 0, \dots, K-1$  **do**

**repeat**

Draw sample batch of pairs  $(x_0^n, x_T^n)_{n \leq N}$   
 Compute  $\mathcal{Y}_0^k(x_0^n) = y_0^n = \mathcal{Z}_{\tilde{\theta}}^k(0, x_0^n)$  and  
 $\mathcal{Y}_T^k(x_T^n) = y_T^n = \mathcal{Z}_{\tilde{\theta}}^k(T, x_T^n)$   
 Sample batch  $(y_t^n)_{n \leq N} \sim \mathbb{W}_{|y_0, y_1}$  using (10)  
 Compute the drift  $s_\theta^k$  using (13) and update  $\theta^k$  by  
 minimizing (11)

**until** convergence

$\theta^{k+1} \leftarrow \theta^k$

**repeat**

Draw sample batch of pairs  $(x_0^n, x_T^n)_{n \leq N}$   
 Compute  $\mathcal{X}_0(x_0^n) = x_0^n + \frac{1}{\beta} s_\theta^{k+1}(0, x_0^n)$  and  
 $\mathcal{X}_T(x_T^n) = x_T^n + \frac{1}{\beta} s_\theta^{k+1}(T, x_T^n)$   
 Update  $\tilde{\theta}^k$  by minimizing (12)

**until** convergence

$\tilde{\theta}^{k+1} \leftarrow \tilde{\theta}^k$

**end for**

**Return**  $\theta^K, \tilde{\theta}^K$

---

4. **Regression step on  $\tilde{\theta}$ .** Once  $\theta^{k+1}$  is obtained, update  $\tilde{\theta}^k$  by minimizing

$$\begin{aligned} \mathcal{L}(\tilde{\theta}^k) = & \mathbb{E}_{x_0 \sim \mu_0, x_T \sim \mu_T} \left[ \|\mathcal{Z}_{\tilde{\theta}}^k(0, \mathcal{X}_0(x_0)) - x_0\|^2 \right. \\ & \left. + \|\mathcal{Z}_{\tilde{\theta}}^k(T, \mathcal{X}_T(x_T)) - x_T\|^2 \right]. \end{aligned} \quad (12)$$

Moreover, using a Gaussian-mixture parametrization of  $v$  from LightSBB-M, we can derive a closed-form expression for the drift  $s_\theta \triangleq s_{v_\theta}$  (Gushchin et al., 2024) as follows:

$$\begin{aligned} s_\theta(t, y) = & \varepsilon \nabla_y \log \mathcal{N}(y \mid 0, \varepsilon(T-t)I_d) \\ & \times \sum_{j=1}^J \alpha_j \mathcal{N}(r_j \mid 0, \varepsilon \Sigma_j) \mathcal{N}(h_j(t, y) \mid 0, A_j^t), \end{aligned} \quad (13)$$

where  $A_j^t \triangleq \frac{t}{\varepsilon(T-t)} I_d + \frac{1}{\varepsilon} \Sigma_j^{-1}$  and  $h_j(t, y) \triangleq \frac{y}{\varepsilon(T-t)} + \frac{1}{\varepsilon} \Sigma_j^{-1} r_j$ .

We also provide in Appendix A alternative algorithms, including a simplification of Algorithm 1 when  $\beta$  is large and Sinkhorn-based solver for the SBB problem.

Note that the regression loss (11) rules out arbitrarily small  $T$  as the target would explode. On the other hand, an excessively large  $T$  drives the noisy marginal  $\mu_T$  to become

almost indistinguishable from  $\mu_0$ , forcing the reverse dynamics to undo an overwhelming amount of noise; this dramatically inflates the variance of the optimal control and deteriorates sample quality. Hence, in practice we choose  $T$  away from extremal values and hence too small  $\beta$ .

Empirically, the proposed alternating procedure converged in a small number of iterations (five in most experiments), consistently yielding stable solutions, despite the absence of a formal convergence proof.

#### 4.2. Inference

Once the drift  $s_\theta^K$  and the transport map  $\mathcal{Z}_\theta^K$  are trained, one can generate new samples from  $\mu_T$  by first computing  $Y_0 = \mathcal{Z}_\theta^K(X_0) \sim \mathcal{Y}_0 \# \mu_0$ , where  $X_0 \sim \mu_0$  is an out-of-sample point. Then, sample  $Y_T \sim \mathcal{Y}_T \# \mu_T$  according to the learned coupling  $\pi_{v_\theta}(Y_T | Y_0)$  given by (5), and recover  $X_T = Y_T + \frac{1}{\beta} s_\theta^K(T, Y_T) \sim \mu_T$ . Alternatively, one could simulate the SDE  $dY_t = s_\theta^K(t, Y_t) dt + \sqrt{\varepsilon} dW_t$ , using a numerical SDE solver (e.g., the Euler–Maruyama scheme), but this approach is generally more time-consuming and introduces additional discretization errors.

Note that the drift  $s_\theta$  defined in (13) is not well-defined at  $t = T$ . Nevertheless, by continuity of  $\phi = \log h$  with respect to time, we can instead approximate  $X_{\tilde{T}} = Y_{\tilde{T}} + \frac{1}{\beta} s_\theta^K(\tilde{T}, Y_{\tilde{T}})$ , where  $\tilde{T} = T - \delta$  for some small  $\delta > 0$ .

## 5. Numerical Experiments

In this section, we present numerical experiments to evaluate the proposed algorithm on both univariate and multivariate datasets. We also provide a comparative analysis against state-of-the-art (SOTA) generative models. In all our experiments, we have used  $T = 1$ .

#### 5.1. Illustrative Examples

We propose to use the SBB framework to transport between two simple distributions. First, we apply SBB between  $\mu_0 = \mathcal{N}(1, 2)$  and  $\mu_T = \mathcal{N}(0, 1)$  with parameters  $\beta = 10$ ,  $K = 5$ , and  $M_{\text{samples}} = 2000$ . Figure 1 displays the trajectories generated by SBB for this case, as well as for a more challenging setting involving heavy-tailed distributions. Indeed, one of the main advantages of SBB compared to the classical SB is that it removes the requirement  $\text{KL}(\mathbb{P} \parallel \mathbb{W}^\varepsilon) < \infty$ . To illustrate this property, we consider the case  $\mu_0 = \delta_0$  and  $\mu_T = \mathcal{T}(2)$ . When the reference marginal at time  $T$  is Gaussian, the KL divergence between  $\mu_T = \mathcal{T}(2)$  and the Wiener measure diverges, since the integrand behaves as  $x^2 p_{\text{Student}}(x) \sim 1/|x|$  for large  $|x|$ , leading to a logarithmic divergence. Consequently, no finite-entropy SB exists between a Dirac initial measure and such a heavy-tailed terminal distribution under a Brownian prior, while

the SBB formulation remains well defined and numerically stable.

#### 5.2. Quantitative Evaluation on Low-Dimensional Datasets

We provide a quantitative evaluation of the proposed SBB method on low-dimensional datasets, namely **8gaussians** and **moons** ( $d = 2$ ), and compare it against several SOTA baselines. These include alternative SB solvers (Gushchin et al., 2024; Shi et al., 2023; Tong et al., 2024b; De Bortoli et al., 2021) and flow-based generative approaches (ODE) (Tong et al., 2024a; Lipman et al., 2023; Liu, 2022). Each model transports 10,000 samples from the source to the target distribution, and performance is assessed using the 2-Wasserstein distance.

The 2-Wasserstein distance between two probability measures  $q_0$  and  $q_1$  on a metric space  $(\mathcal{X}, d)$  is defined as

$$\mathcal{W}_2(q_0, q_1) = \left( \inf_{\gamma \in \Gamma(q_0, q_1)} \int_{\mathcal{X} \times \mathcal{X}} \|x - y\|^2 d\gamma(x, y) \right)^{1/2},$$

where  $\Gamma(q_0, q_1)$  denotes the set of all couplings of  $q_0$  and  $q_1$ . In our experiments, we aim to minimize this distance between samples generated by the SBB model and those drawn from the ground-truth distribution. All results are averaged over five seeds, and we report both the mean and standard deviation. As shown in Table 1, the proposed SBB framework consistently achieves the lowest  $\mathcal{W}_2$  distances across all benchmark tasks. It outperforms both SB-based methods (e.g., LightSBB-M) and diffusion/flow-based baselines, yielding on average a  $\sim 19\%$  improvement in transport accuracy, while reducing the variance of the results. These results highlight the efficiency and stability of SBB in modeling complex multimodal and non-Gaussian distributions such as the *moons*  $\rightarrow$  *8-gaussians* task. Note that FM is incompatible with the latter as it requires a Gaussian source distribution.

We further analyze the influence of the parameter  $\beta$  on the transport quality, ranging from  $\beta = 10$  up to  $\beta = \infty$  that is the SB regime. Figure 2 shows that  $\mathcal{W}_2$  distances decrease rapidly as  $\beta$  increases from 10 to 100, except for the  $\mathcal{N} \rightarrow$  8gaussians that keeps increasing, with optimal performance achieved between  $\beta = 10$  and 100 across both datasets. Beyond  $\beta = 100$ , performance slightly degrades, suggesting an intermediate  $\beta$  value provides the best trade-off between the drift and the volatility.

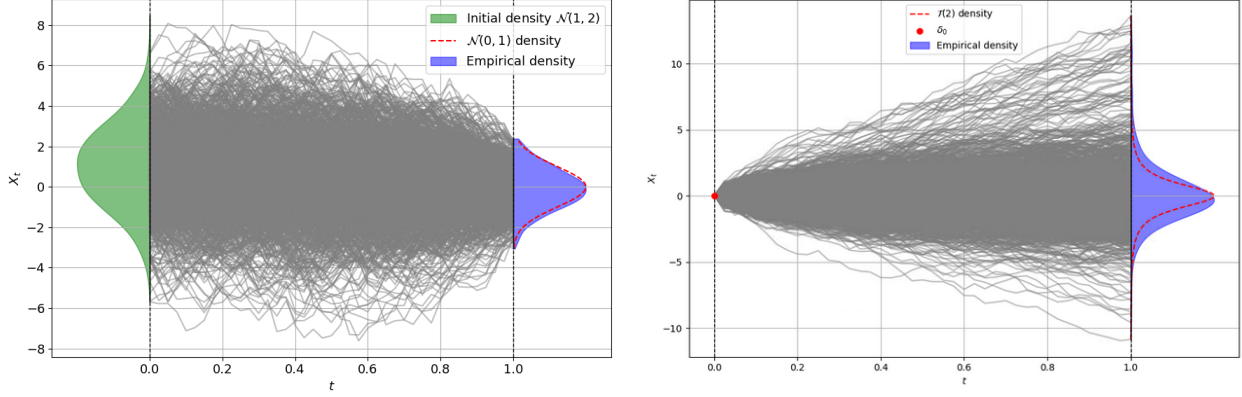


Figure 1. Transport interpolation using SBB:  $\mathcal{N}(1, 2) \rightarrow \mathcal{N}(0, 1)$  (left) and  $\delta_0 \rightarrow \mathcal{T}(2)$  (right).

Table 1. 2-Wasserstein distances ( $\mathcal{W}_2$ ) on synthetic datasets (lower is better). The best results are highlighted in **bold**. \*Indicates results taken from (Tong et al., 2024b)

Algorithm	$\mathcal{W}_2$ (↓)		
	$\mathcal{N} \rightarrow 8\text{gaussians}$	$\text{moons} \rightarrow 8\text{gaussians}$	$\mathcal{N} \rightarrow \text{moons}$
[SF] <sup>2</sup> M-Exact*	0.275±0.058	0.726±0.137	0.124±0.023
[SF] <sup>2</sup> M-I*	0.393±0.054	1.482±0.151	0.185±0.028
DSBM-IPF*	0.315±0.079	0.812±0.092	0.140±0.006
DSBM-IMF*	0.338±0.091	0.838±0.098	0.144±0.024
DSB*	0.411±0.084	0.987±0.324	0.190±0.049
LightSBB-M	0.339±0.099	0.295±0.051	0.201±0.042
<b>SBB (ours)</b>	<b>0.241±0.083</b>	<b>0.201±0.034</b>	<b>0.109±0.014</b>
OT-CFM*	0.303±0.043	0.601±0.027	0.130±0.016
SB-CFM*	2.314±2.112	0.843±0.079	0.434±0.594
RF*	0.421±0.071	1.525±0.330	0.283±0.045
I-CFM*	0.373±0.103	1.557±0.407	0.178±0.014
FM*	0.343±0.058	—	0.209±0.055

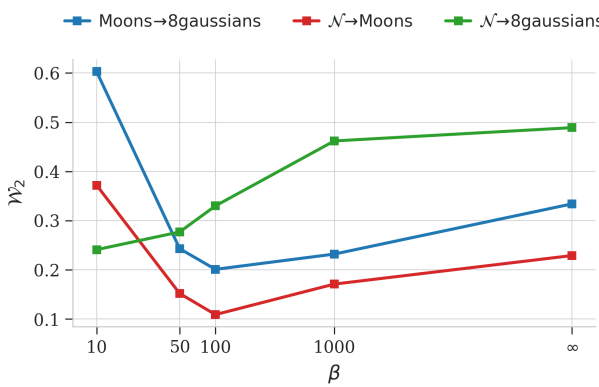


Figure 2. Evolution of the 2-Wasserstein distance  $\mathcal{W}_2$  for different values of  $\beta$  on each datasets.

## 6. Qualitative Evaluation on Unpaired Image-to-Image Translation

To evaluate the generative capabilities of our model we consider the task of unpaired image-to-image translation (Zhu et al., 2017) on subsets of the FFHQ dataset at a reso-

lution of  $1024 \times 1024$  pixels (Karras et al., 2019). The source distribution  $p_0$  comprises adult faces, while the target distribution  $p_T$  consists of child faces. Since the two domains are not paired, we adopt a cycle-consistent framework in the latent space of an Adversarial Latent AutoEncoder (ALAE) (Pidhorskyi et al., 2020). Each image  $\mathbf{x} \in \mathbb{R}^{3 \times 1024 \times 1024}$  is first encoded by the *pretrained* ALAE encoder  $E : \mathbb{R}^{3 \times 1024 \times 1024} \rightarrow \mathbb{R}^{512}$ , producing a latent code  $\mathbf{z} = E(\mathbf{x}) \in \mathbb{R}^{512}$ . Then, we train our SBB framework in that latent space, and decode the final latent output using the *pretrained* ALAE decoder  $D : \mathbb{R}^{512} \rightarrow \mathbb{R}^{3 \times 1024 \times 1024}$ , yielding the translated images. This setup allows us to assess the fidelity of the generated child faces and the preservation of identity-related attributes without requiring paired supervision.

Figure 3 compares our SBB framework with the usual SB approach using the LightSBB-M baseline across several  $(\beta, \varepsilon)$  settings. For the low-noise regime  $\varepsilon = 0.1$ , SBB with small  $\beta$  (e.g.,  $\beta = 1, 10$ ) attains higher visual quality and better fidelity than LightSBB-M, as some images are clearly not of children. Moreover, when the noise level is increased to  $\varepsilon = 1$ , where classical SB exhibits high variance, we observe that small  $\beta$  values lead to greater diversity in the generated outputs. Finally, we also demonstrate that for large values of  $\beta$  (i.e.,  $\beta = 100$ ), the behavior closely matches that of the standard SB, in agreement with the theoretical predictions.

We then propose the experiment illustrated in Figure 4, which generates a child image directly from noise. Unlike conventional diffusion models that rely on a backward-forward sampling (Song & Ermon, 2019; Song et al., 2021) scheme, our approach proceeds in a single forward pass, thereby avoiding the costly reverse diffusion step and error accumulation. We also present the comparison between the  $Y$  and  $X$  process, where we observe that the inverse sample  $X_T$  significantly improves sample quality and corrects potential errors of  $Y_T$ . This improvement is evident both in terms of visual fidelity and distributional alignment, as  $Y_T$  does not always give child images.

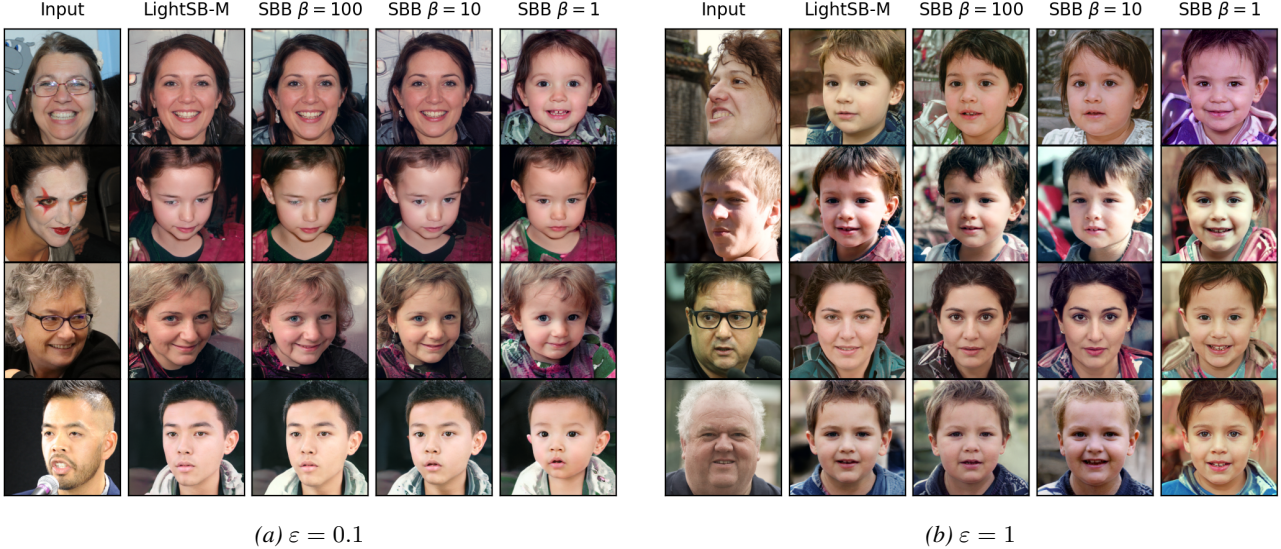


Figure 3. Comparison between our framework SBB and the benchmark LightSB-M. The left column shows the input image.

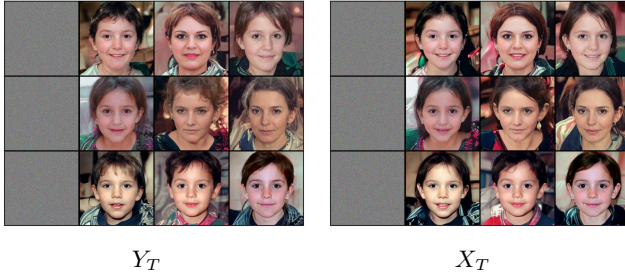


Figure 4. Comparison between  $Y_T$  and  $X_T$  (right) with  $\beta = 5$ . The left column shows the input image, and three representative samples are reported for each method.

Finally, Figure 5 depicts the complete pipeline from the source distribution  $X_0 \sim p_0$  to the target distribution  $X_1 \sim p_1$  together with the underlying  $Y$ -process defined by our framework. The intermediate states  $Y_t$  are obtained via bridge matching Equation (10) between the endpoints  $Y_0$  and  $Y_T$ . Note that this bridging occurs on the  $Y$  process, not on  $X$ , since  $Y$  is a SB



Figure 5. Trajectory from  $X_0 \sim p_0$  to  $X_1 \sim p_1$  with the underlying  $Y$  process.

## 7. Conclusion

**Potential impact.** Our primary contribution is an algorithm that solves the SBB problem for generative modeling. Building on existing methods for the classical SB, we derive an efficient procedure to compute the optimal transport plan

$\mathbb{P}^{SBB}$ . The framework includes a tunable parameter  $\beta$  that balances drift and volatility; we empirically demonstrate how  $\beta$  impacts the sample diversity and fidelity. By incorporating stochastic volatility, the method can accommodate a broader class of target distributions—including those with heavy tails—beyond the restrictive assumptions of the standard SB. Consequently, the generated synthetic data exhibit greater variability while maintaining high fidelity as governed by  $\beta$ .

**Limitations and future work.** Computing  $\mathbb{P}^{SBB}$  requires iterating over the transport map, which can be computationally demanding. In our experiments we limited the iteration count to  $K = 5$  as it seems to converge, yet the algorithm’s convergence has not been formally established. Future research should (i) develop tighter iteration-complexity bounds, (ii) provide a rigorous convergence proof, and (iii) explore acceleration techniques (e.g., stochastic approximations or multigrid schemes) to reduce the number of required iterations. A natural extension of the method is to apply the SBB framework to time-series data. While the SB problem has already been employed for sequential data (Hamdouche et al., 2023; Alouadi et al., 2025), the stochastic-volatility extension proposed here has not. Incorporating the controlled volatility could markedly improve the realism of generated time series, particularly in financial domains where heteroskedasticity is prevalent.

## References

Alouadi, A., Barreau, B., Carlier, L., and Pham, H. Robust time series generation via schrödinger bridge: a comprehensive evaluation. In *International Conference on AI in Finance*, 2025.

Alouadi, A., Henry-Labordère, P., Loeper, G., Mazhar, O., Pham, H., and Touzi, N. A pde derivation of the schrödinger–bass bridge, 2026.

Backhoff, J., Loeper, G., and Obloj, J. Geometric martingale benamou–brenier transport and geometric bass martingales. *Proceedings of the American Mathematical Society*, 2025.

Bass, R. F. Skorokhod imbedding via stochastic integrals. *Séminaire de Probabilités*, 1983.

De Bortoli, V., Thornton, J., Heng, J., and Doucet, A. Diffusion schrödinger bridge with applications to score-based generative modeling. In *Advances in Neural Information Processing Systems*, 2021.

Föllmer, H. Random fields and diffusion processes. 1988.

Gushchin, N., Kholkin, S., Burnaev, E., and Korotin, A. Light and optimal schrödinger bridge matching. In *Proceedings of the 41st International Conference on Machine Learning*, 2024.

Hamdouche, M., Henry-Labordere, P., and Pham, H. Generative modeling for time series via schrödinger bridge, 2023.

Karras, T., Laine, S., and Aila, T. A style-based generator architecture for generative adversarial networks. In *Proceedings of the IEEE/CVF Conference on Computer Vision and Pattern Recognition (CVPR)*, pp. 4401–4410, 2019.

Korotin, A., Gushchin, N., and Burnaev, E. Light schrödinger bridge. In *International Conference on Learning Representations*, 2024.

Léonard, C. A survey of the schrödinger problem and some of its connections with optimal transport. *Discrete & Continuous Dynamical Systems-A*, 2014.

Lipman, Y., Chen, R. T. Q., Ben-Hamu, H., Nickel, M., and Le, M. Flow matching for generative modeling. In *International Conference on Learning Representations*, 2023.

Liu, Q. Rectified flow: A marginal preserving approach to optimal transport. *arXiv preprint arXiv:2209.14577*, 2022.

Peyré, G. and Cuturi, M. Computational optimal transport. *Foundations and Trends in Machine Learning*, 2019.

Pidhorskyi, S., Adjeroh, D. A., and Doretto, G. Adversarial latent autoencoders. In *Proceedings of the IEEE/CVF Conference on Computer Vision and Pattern Recognition (CVPR)*, pp. 14104–14113, 2020.

Schrödinger, E. Sur la théorie relativiste de l'électron et l'interprétation de la mécanique quantique. *Annales de l'Institut Henri Poincaré*, 1932.

Shi, Y., De Bortoli, V., Campbell, A., and Doucet, A. Diffusion schrödinger bridge matching. In *Advances in Neural Information Processing Systems*, 2023.

Song, Y. and Ermon, S. Generative modeling by estimating gradients of the data distribution. In *Advances in Neural Information Processing Systems*, 2019.

Song, Y., Sohl-Dickstein, J., Kingma, D. P., Kumar, A., Ermon, S., and Poole, B. Score-based generative modeling through stochastic differential equations. In *International Conference on Learning Representations (ICLR)*, 2021.

Tong, A., Fatras, K., Malkin, N., Huguet, G., Zhang, Y., Rector-Brooks, J., Wolf, G., and Bengio, Y. Improving and generalizing flow-based generative models with minibatch optimal transport. *Transactions on Machine Learning Research*, 2024a.

Tong, A., Malkin, N., Fatras, K., Atanackovic, L., Zhang, Y., Huguet, G., Wolf, G., and Bengio, Y. Simulation-free schrödinger bridges via score and flow matching. In *Proceedings of The 27th International Conference on Artificial Intelligence and Statistics (AISTATS)*, 2024b.

Zhu, J.-Y., Park, T., Isola, P., and Efros, A. A. Unpaired image-to-image translation using cycle-consistent adversarial networks. In *Proceedings of the IEEE International Conference on Computer Vision*, pp. 2223–2232, 2017.

## A. Exploring Alternative Algorithms

In this section, we are exploring other potential algorithms to solve the SBB problem.

### A.1. LightSBB-M for $\beta$ Large

We recall that the objective of Algorithm 1 is to estimate both the drift of the process  $Y$  and the transport map  $\mathcal{Y}_t(X_t) = X_t - \frac{1}{\beta} \varepsilon \nabla_y \log h_t^*(\mathcal{Y}_t(X_t))$  for  $t \in [0, T]$ . One may notice that for large  $\beta$ , we can make the following approximation of the transport map:

$$\mathcal{Y}_t(X_t) = X_t - \frac{1}{\beta} \varepsilon \nabla_y \log h_t^*(\mathcal{Y}_t(X_t)) \simeq X_t - \frac{1}{\beta} \varepsilon \nabla_y \log h_t^*(X_t) \quad (14)$$

Approximation 14 hence provides an explicit expression, given the drift, of the transport map and avoid computing the inverse of  $\mathcal{X}$ . One can simply sample from  $\mathcal{Y}_t \# \mu_t$ , at iteration  $k$ , using

$$\begin{cases} \mathcal{Y}_0^k(x_0) = y_0 = x_0 - \frac{1}{\beta} \log s_\theta^k(0, x_0), \\ \mathcal{Y}_T^k(x_T) = y_T = x_T - \frac{1}{\beta} \log s_\theta^k(T, x_T) \end{cases} \quad (15)$$

Then, Algorithm 1 simply becomes as described in Algorithm 2.

---

#### Algorithm 2 LightSBB-M for $\beta$ large

---

**Input:** Samples  $(x_0^m, x_T^m)_{m \leq M} \sim (\mu_0, \mu_T)$ ,  $\theta = \{\alpha_j, \mu_j, \Sigma_j\}_{j \leq J}$ ,  $\beta > 0$  large,  $K > 0$

**Initialization:** Start with  $\mathcal{Y}^0 = I_d$

**for**  $k = 0, \dots, K - 1$  **do**

**repeat**

        Draw sample batch of pairs  $(x_0^n, x_T^n)_{n \leq N}$

        Compute  $\mathcal{Y}_0^k(x_0^n) = y_0^n$  and  $\mathcal{Y}_T^k(x_T^n) = y_T^n$  using (15)

        Sample batch  $(y_t^n)_{n \leq N} \sim \mathbb{W}_{|y_0, y_1}$  using (10)

        Compute the drift  $s_\theta^k$  using (13) and update  $\theta^k$  by minimizing (11)

**until** convergence

$\theta^{k+1} \leftarrow \theta^k$

**end for**

**Return**  $\theta^K$

---

Once  $s_\theta^K$  is trained, one can sample similarly as before. First, compute  $Y_0 = X_0 - \frac{1}{\beta} \log s_\theta^K(0, X_0) \sim \mathcal{Y}_0 \# \mu_0$  where  $X_0 \sim \mu_0$  is an out-of-sample point. Then, sample  $Y_T \sim \mathcal{Y}_T \# \mu_T$  according to the learned coupling  $\pi_{v_\theta}(Y_T | Y_0)$  given by (5), and recover  $X_T = Y_T + \frac{1}{\beta} s_\theta^K(T, Y_T) \sim \mu_T$ .

This approximation eliminates the need to learn an explicit transport map, which reduces computational cost and mitigates the accumulation of approximation errors during training.

### A.2. Sinkhorn-based Algorithm

We introduce a Sinkhorn-based algorithm that iteratively updates the potential function  $\phi$ , setting  $\varepsilon = 1$  for simplicity of notation. The algorithm proceeds as follows, starting from  $\phi^0 = 0$ , for all  $0 \leq k \leq K$ :

1. Compute  $h_0^k(y) = \mathbb{E}_{\mathcal{N}(0, T)}(e^{\phi^k(y+Z)}) \simeq \frac{1}{N} \sum_{i=1}^N e^{\phi^k(y+Z_i)}$  with  $(Z_i)_{i \leq N} \sim \mathcal{N}(0, T)$  i.i.d.
2. Compute  $\mathcal{Y}_0^k(x) = \arg \min_{y \in \mathbb{R}^d} \left[ \log h_0^k(y) + \frac{\beta}{2} \|x - y\|^2 \right]$  for  $x \sim \mu_0$ . This can be achieved either via grid search, or approximately (for large  $\beta$ ) using  $\mathcal{Y}_0^k(x) \simeq x - \frac{1}{\beta} \nabla_y \log h_0^k(x)$ , where  $\nabla_y \log h_0^k(x)$  is obtained by interpolating  $\log h_0^k$  and estimating its gradient via finite differences for all  $x \sim \mu_0$ .
3. Compute  $\mathcal{Y}_T^k(x) = \arg \min_{y \in \mathbb{R}^d} \left[ \phi^k(y) + \frac{\beta}{2} \|x - y\|^2 \right]$  for  $x \sim \mu_T$ . Similarly, this can be done either through grid

search or, when  $\beta$  is large, by approximating  $\mathcal{Y}_T^k(x) \simeq x - \frac{1}{\beta} \nabla_y \phi^k(x)$ , where the gradient is computed from an interpolated version of  $\phi^k$  using finite differences.

4. Compute  $h_T^{k+1}(y) = e^{\phi^{k+1}(y)} = \frac{\mathbb{E}_{\mu_T} \left( \delta_{\mathcal{Y}_T^k(x_T)}(y) \right)}{\mathbb{E}_{\mu_0} \left( \frac{\mathcal{N}_{\mathcal{Y}_0^k(x_0), T}(y)}{h_0^k(\mathcal{Y}_0^k(x_0))} \right)}$  via Monte Carlo estimation using samples from  $\mu_T$  and  $\mu_0$ .
5. Update  $\phi^{k+1} = \log h_T^{k+1}$ .

After convergence,  $\phi^* \simeq \phi^K$ , one can simulate the diffusion  $dY_t = \nabla_y \log h_t^K(Y_t) dt + dW_t$  starting from  $Y_0 \sim \mathcal{Y}_0^K \# \mu_0$  obtained in step 2, with  $h_t^K = h_T^K * \mathcal{N}_{T-t}$  computed on a grid and interpolated to estimate its score via finite differences. Note that this approach is computationally demanding and does not scale well to high-dimensional settings due to: (i) the need for interpolation, (ii) the grid search procedure, and (iii) the estimation of the density of  $\mathcal{Y}_T^k \# \mu_T$  in the numerator of step 4, which can be performed using kernel regression methods.

Alternatively, one may directly simulate the process  $X$  as follows:

- **Compute**  $h_t^K(\cdot)$  as in step 4, using  $\mathcal{Y}_T^K(\cdot)$  and  $\mathcal{Y}_0^K(\cdot)$ .
- **Compute**  $\mathcal{Y}_t^K(\cdot)$  as in step 3.
- **Compute the optimal drift and volatility controls.** The expressions of the optimal drift  $\alpha^K$  and volatility  $\sigma^K$  at time  $t$  are given by:

$$\begin{cases} \alpha^K(t, x) = \nabla_y \log h_t^K(\mathcal{Y}_t^K(x)) = \frac{\nabla_y h_t^K(\mathcal{Y}_t^K(x))}{h_t^K(\mathcal{Y}_t^K(x))}, \\ \sigma^K(t, x) = I_d + \frac{1}{\beta} \nabla_y^2 \log h_t^K(\mathcal{Y}_t^K(x)) = I_d + \frac{1}{\beta} \left( \frac{\nabla_y^2 h_t^K(\mathcal{Y}_t^K(x))}{h_t^K(\mathcal{Y}_t^K(x))} - \frac{\nabla_y h_t^K(\mathcal{Y}_t^K(x)) \nabla_y h_t^K(\mathcal{Y}_t^K(x))^T}{h_t^K(\mathcal{Y}_t^K(x))^2} \right) \end{cases}$$

where the derivatives are obtained from the interpolated version of  $h_t^K(\cdot)$  using finite differences.

We propose to evaluate this approach by transporting between measures  $\mu_0$  and  $\mu_T$  for which the optimal drift and volatility are known. As an illustrative example, consider  $\mu_0 = \delta_0$  and  $\mu_T = \mathcal{N}(0, T)$ . In this case, the optimal drift and volatility are given by  $\alpha_0^* = 0$  and  $\sigma_0^* = I_d$ , since  $X_T = \alpha_0^* T + \sigma_0^* W_T = 0 + I_d \times \mathcal{N}(0, T) \sim \mathcal{N}(0, T)$ . We perform the experiment using 2000 real samples drawn from  $\mathcal{N}(0, T)$  with parameters  $T = 1$ ,  $\beta = 1$ ,  $K = 20$ ,  $N^\pi = 1$ ,  $N = 1$ , and initialization  $\phi^0(y) = \frac{y^2}{4}$ . The estimated values are  $\hat{\alpha}_0 = 0.002$  and  $\hat{\sigma}_0 = 1.001$ . Figure 6 shows the estimated drift and volatility obtained with SBB across all time steps  $t \in [0, T]$ , along with the empirical cumulative distribution function (ECDF) computed from both real and generated samples.

We also present in Figure 7 illustrative toy examples in one dimension, demonstrating the behavior of the alternative Sinkhorn algorithm for transporting between different probability measures. In these experiments, we set  $\beta = 10$ ,  $K = 20$ , and  $N^\pi = 40$ , corresponding to the number of time steps in the Euler scheme. For the density estimation in step 4, we employ the following kernel function:

$$K_\lambda(x) = \frac{1}{\lambda^d} \left( 1 - \left\| \frac{x}{\lambda} \right\|^2 \right)^2 \mathbf{1}_{\{\|x\| < \lambda\}}, \quad x \in \mathbb{R}^d,$$

where  $\lambda = 0.3$  denotes the kernel bandwidth.

## B. Experimental Setup

All experiments were conducted using a single NVIDIA A100 SXM4 40 GB GPU. The parameters used throughout this study, unless otherwise stated, are summarized in Table 2.

Under this setup, training completes in under 10 minutes for 2-d tasks, and inference is inexpensive (less than 1 minutes for 10,000 samples). For image translation, the computational cost of LightSBB-M is comparable to that of LightSB-M, as the additional overhead arises only from the outer-loop iterations ( $K = 5$ ), which we found to be negligible relative to the cost of training the score network.

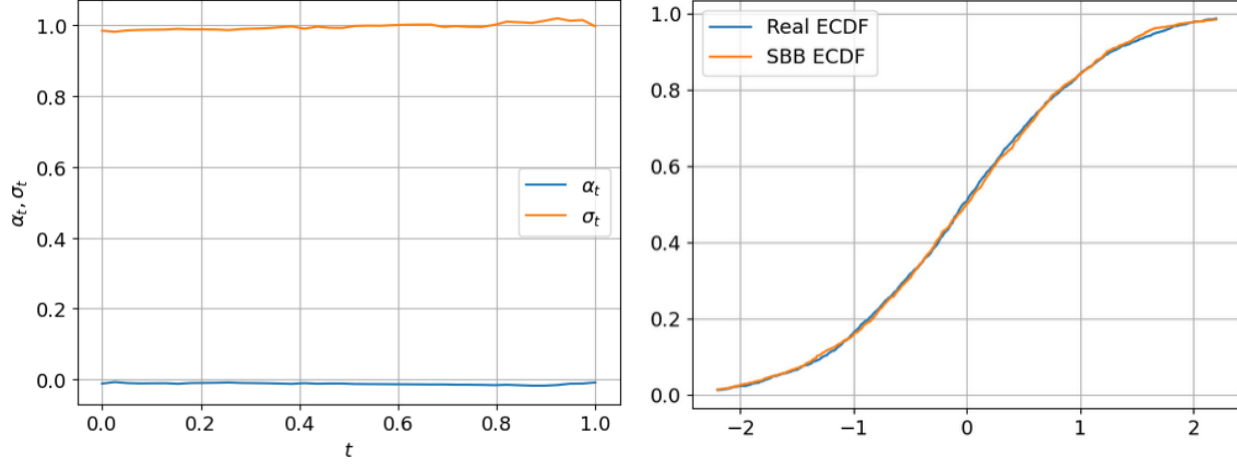


Figure 6. Estimated optimal drift/volatility over time (left) and Empirical CDF comparison between real and SBB-generated samples (right)

Table 2. Table of parameters and their values

$K$	$T$	$\tilde{T}$	$n_{epoch}$	Batch Size	$lr$
5	1	0.99	15000	512	$10^{-3}$

## B.1. Model Architecture

The transport map  $\mathcal{Z}_\theta$  is defined by a simple multilayer perceptron (MLP). The network takes as input the time  $t \in \mathbb{R}$  and the state  $x \in \mathbb{R}^d$ . Each input is first processed by a feed-forward network (FFN) comprising a linear layer, a normalization layer, a GELU activation function, and a final linear layer. This projects the inputs into latent spaces of dimension  $t_{\text{model}}$  and  $d_{\text{model}}$ , respectively. The resulting embeddings are then concatenated and passed through a subsequent FFN with a similar structure, which maps the combined representation back to the original space  $\mathbb{R}^d$ .

## B.2. Quantitative Evaluation Setup

For these experiments, we set the model hyperparameters to  $t_{\text{model}} = 8$  and  $d_{\text{model}} = 32$  with  $J = 50$  potentials in the Gaussian mixture. To remain consistent with the setup in (Tong et al., 2024b), we use  $\varepsilon = 1$  for all datasets, except for  $\text{moons} \rightarrow 8 \text{ gaussians}$ , where we set  $\varepsilon = 5$ . Moreover, we use  $K = 25$  iterations for the  $\mathcal{N} \rightarrow \text{moons}$  dataset, as this setting provides more stable and consistent results. Table 3 reports the 2-Wasserstein distances ( $\mathcal{W}_2$ ) obtained for varying values of  $\beta$  across all considered datasets.

Table 3. 2-Wasserstein distances ( $\mathcal{W}_2$ ) on synthetic datasets (lower is better) for different  $\beta$  values. The best results are highlighted in **bold**.

$\beta$	$\mathcal{W}_2 (\downarrow)$		
	$\mathcal{N} \rightarrow 8\text{gaussians}$	$\text{moons} \rightarrow 8\text{gaussians}$	$\mathcal{N} \rightarrow \text{moons}$
1	$4.103 \pm 1.247$	$2.312 \pm 1.089$	$0.927 \pm 0.743$
10	<b><math>0.241 \pm 0.083</math></b>	$0.603 \pm 0.048$	$0.372 \pm 0.032$
50	$0.277 \pm 0.096$	$0.243 \pm 0.029$	$0.152 \pm 0.024$
100	$0.330 \pm 0.077$	<b><math>0.201 \pm 0.034</math></b>	<b><math>0.109 \pm 0.014</math></b>
1000	$0.462 \pm 0.091$	$0.232 \pm 0.025$	$0.171 \pm 0.037$
$\infty$	$0.489 \pm 0.084$	$0.334 \pm 0.058$	$0.229 \pm 0.019$

Figure 8 visualizes the transport results for all  $\beta$  values. In each subplot, the initial distribution  $\mu_0$  is shown in *blue*, and the

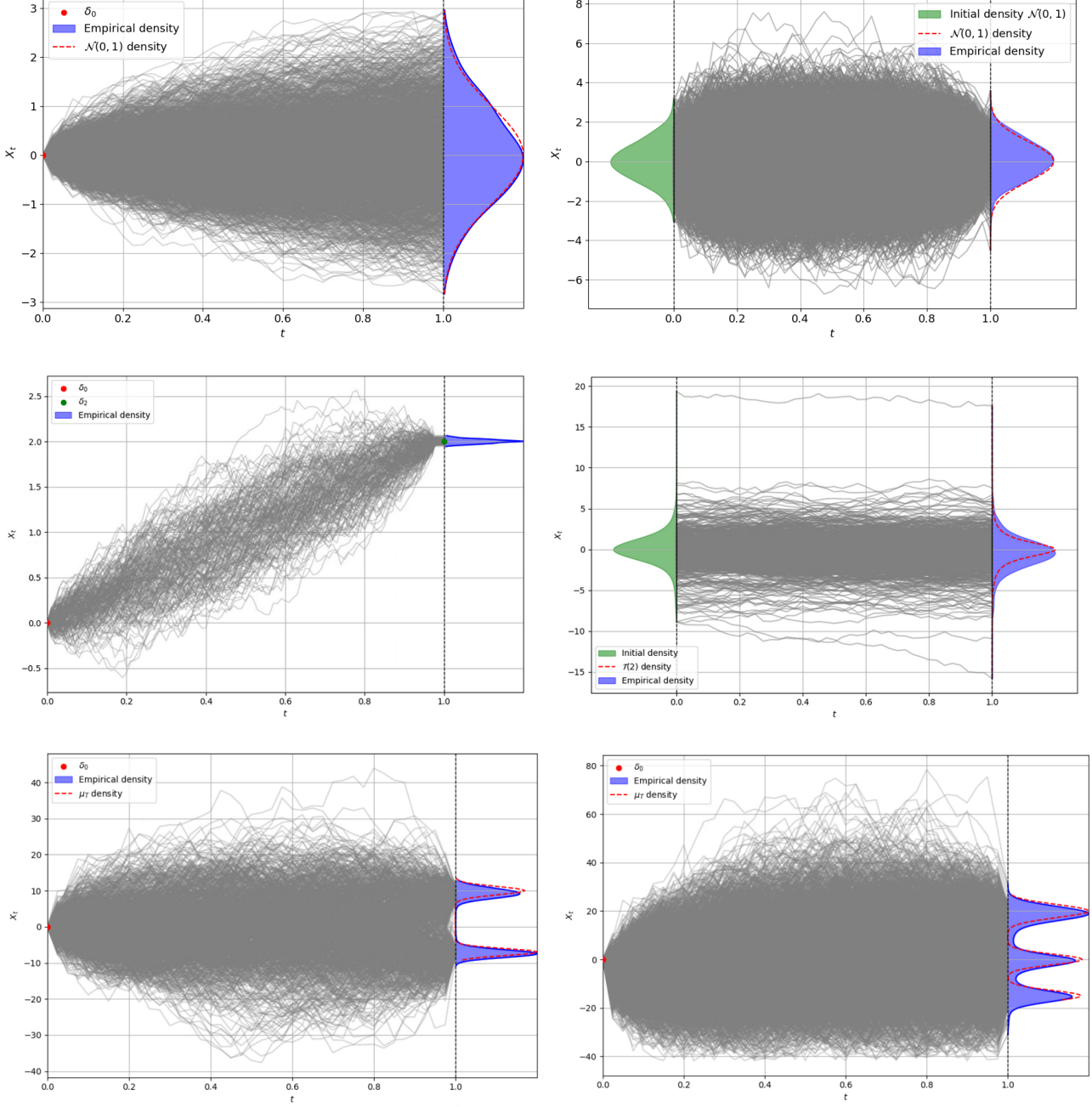


Figure 7. Transport interpolation examples. (Top)  $\delta_0 \rightarrow \mathcal{N}(0, 1)$  and  $\mathcal{N}(0, 1) \rightarrow \mathcal{N}(0, 1)$ . (Middle)  $\delta_0 \rightarrow \delta_2$  and  $\mathcal{T}(2) \rightarrow \mathcal{T}(2)$ . (Bottom)  $\delta_0 \rightarrow$  multimodal distribution.

transported distribution  $\mu_T$  is shown in *orange*. For the smallest tested value,  $\beta = 1$ , the algorithm fails to converge. This behavior can be attributed to the violation of the required condition  $\beta > \frac{1}{T}$ , which is not satisfied when  $T = 1$ .

### B.3. Unpaired Image-to-Image Translation Setup

For unpaired image-to-image translation, we closely follow the experimental setup in (Gushchin et al., 2024). The dataset consists of 70,000 labeled images, of which 60,000 were used for training and 10,000 for testing. The model hyperparameters were set to  $t_{\text{model}} = 32$  and  $d_{\text{model}} = 128$ , with  $J = 10$  potentials in the Gaussian mixture. This results in a drift model with approximately 2.6 million parameters, and a transport map estimator with 100,000 parameters. Training

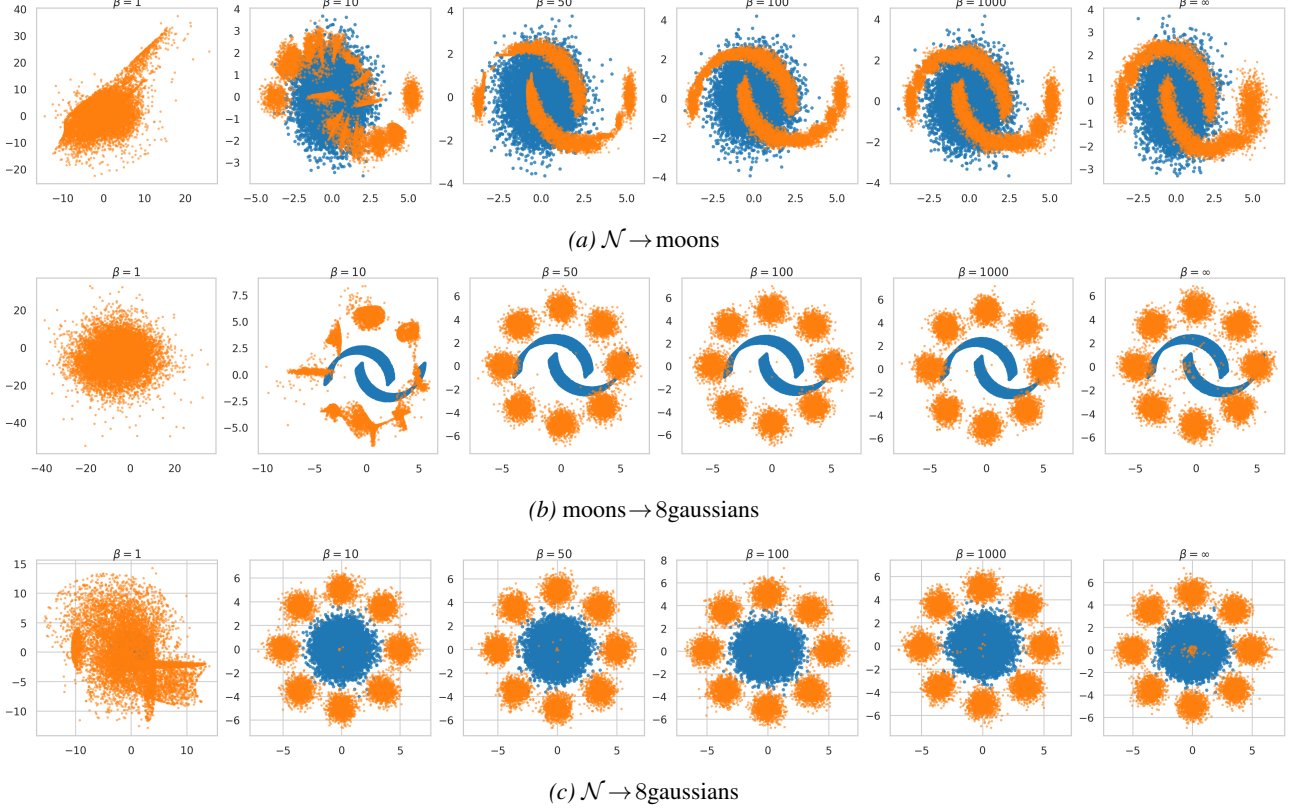
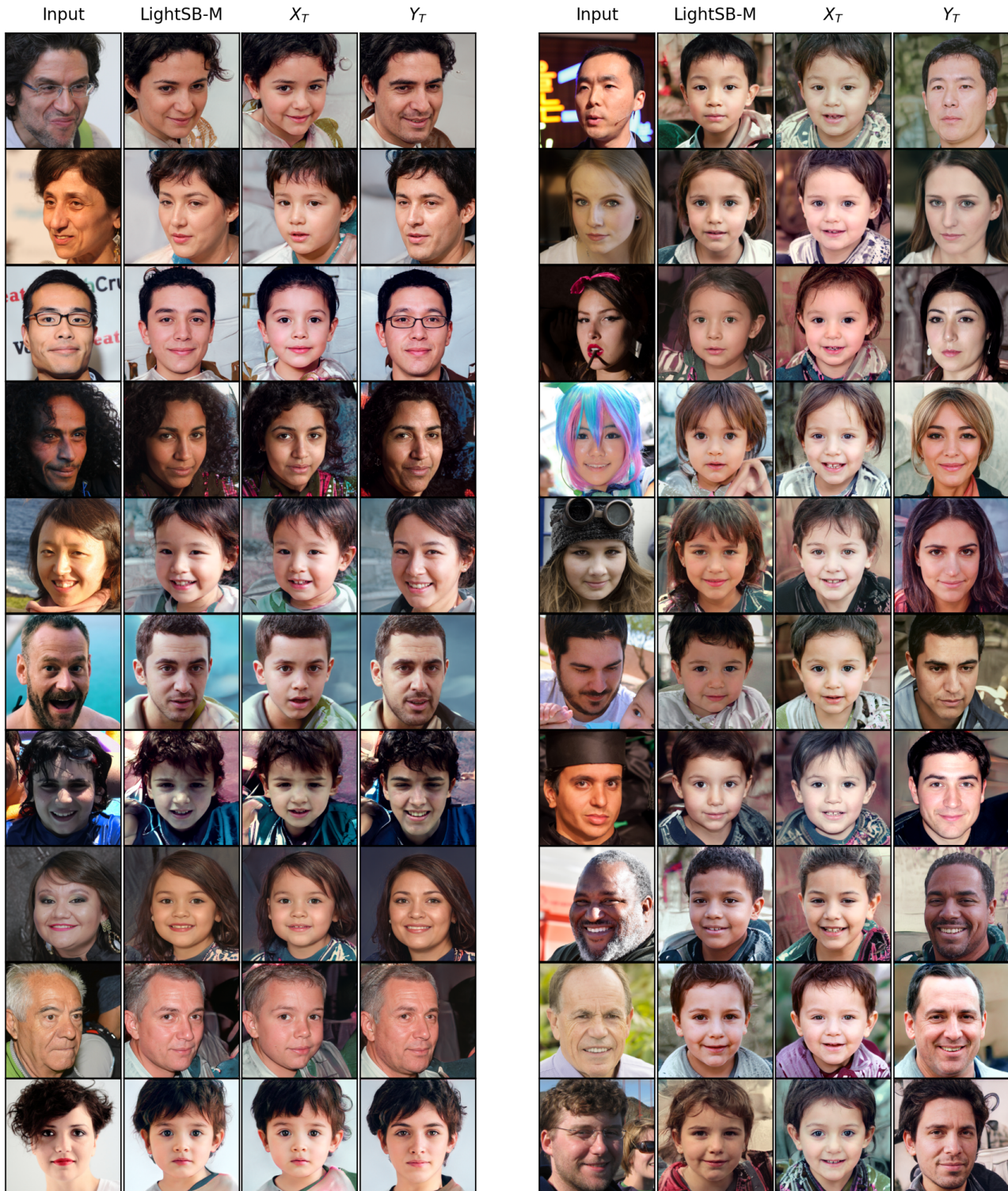


Figure 8. Transport results across datasets for different  $\beta$  values. Initial distributions  $\mu_0$  are shown in blue, and transported distributions  $\mu_T$  in orange.

took under 5 minutes, and inference on 10 input images required less than 1 minute.

Our implementation builds upon the code provided by (Gushchin et al., 2024), available at: <https://github.com/SKholkin/LightSB-Matching/tree/main>. Figure 9 provides additional examples of our method, showing both  $X_T$  and  $Y_T$  for  $\beta = 1$  and  $\varepsilon \in \{0.1, 1\}$ , with LightSB-M used as the baseline for comparison.


 (a)  $\varepsilon = 0.1$ 

 (b)  $\varepsilon = 1$ 

Figure 9. Additional examples for unpaired image-to-image translation using LightSBB-M as the baseline. Results show both  $X_T$  and  $Y_T$  from SBB for  $\beta = 1$  and  $\varepsilon \in \{0.1, 1\}$ .